Pergamon

Int. J. Heat Mass Transfer. Vol. 37, Suppl. 1, pp. 395–402, 1994

0017-9310/94 $6.00 + 0.00

0017-9310(93)E0071-N

Numerical and experimental results for coupled heat and mass transfer between a desiccant film and air in cross-flow

M. S. PARK, JOHN R. HOWELL, GARY C. VLIET and JOHN PETERSON

Department of Mechanical Engineering and Center for Energy Studies, University of Texas at Austin, Austin, TX 78712-1063, U.S.A.

Abstract—Heat and mass transfer with a uniformly distributed falling liquid desiccant film in a cross-flow parallel plate gas–liquid heat exchanger is predicted, and the results compared with experiment. The process air is in cross-flow over the desiccant film. Refrigerant flows through the heat exchanger tubes and removes the heat of absorption for dehumidification and supplies the heat for regeneration. The governing equations, boundary conditions, and interfacial equilibrium conditions for the concentration, temperature and pressure are presented. The problem is more complex than for cocurrent or countercurrent flow, as it is fully three-dimensional.

INTRODUCTION

IN RECENT years extensive research has been performed on falling film flow because it has found wide application in modern process industries involving heat and mass transfer.

The operation of a desiccant system such as an absorber/evaporator is made possible by the property of desiccants of attracting and holding water vapor from the surrounding air at low temperatures and releasing water to air at high temperatures. Here, we examine liquid desiccants, in particular triethylene glycol (TEG) [1].

The exchange of water vapor between air and liquid desiccant depends on the relative magnitude of water vapor pressure in the air and at the surface of the liquid desiccant, respectively. When a desiccant (TEG solution) is brought into contact with air with a given water vapor partial pressure, as shown in Fig. 1, water will be transferred from the air to a TEG solution that has temperature below T^* and in the reverse direction for TEG solution temperatures greater than T^*. Thus, at low TEG solution temperatures, dehumidification of the air will take place in an absorption process, while at high TEG solution temperatures the water content of the TEG solution will be reduced in a desorption (regeneration) process.

Liquid films are characterized by a large interfacial area per unit volume with a simple geometrical configuration. A special advantage is the thinness of the liquid film, which allows the amount of liquid circulation to be small while keeping the heat and mass transfer rates high. High gas flow rates can be accommodated during cocurrent or crosscurrent flow of gas and liquid film with comparatively small pressure drops.

The phenomenon of flooding poses a problem and limits the use of countercurrent flow. In Ameringer [2] it was found that even at moderately low TEG flow rates in a falling film subject to air in counterflow, the TEG formed large droplets that would cling to the bottom of the fins. These drops would join together to form sheets of TEG across large portions of the bottom of each fin-tube unit. The sheets effectively blocked the air flow.

In this study we have performed a detailed numerical analysis of the heat and mass transfer between a falling desiccant film on a vertical plate and air in cross-flow by simultaneously solving the conservation equations in the liquid film and air stream, subject to boundary and interfacial matching conditions. We have compared the numerical predictions with experimental results.

LITERATURE REVIEW

Fulford [3] presented a review on falling liquid films both for laminar and turbulent films. Olbrich and Wild [4] solved the convective–diffusion equation for various flow geometries that have a certain degree of symmetry. The same kind of problem was treated by Tamir and Taitel [5], but they considered thermodynamic nonequilibrium at the gas–liquid interface by adding a constant interfacial resistance.

Rotem and Neilson [6] analyzed low Peclet number film flow by including the axial diffusion term and found that for most practical cases it is negligible. Murty and Sastri [7] studied analytically the problem of accelerating falling liquid films of the Newtonian type by taking into account the interfacial drag. In Grigor'eva and Nakoryakov [8], the problem is solved analytically for an isothermal wall and a film velocity that is uniform over the film thickness. This assumption overestimates the bulk temperature and concentration of the liquid. In Nakoryakov and Gri-

NOMENCLATURE

C	concentration of water in TEG solution, [kg water (kg solution)$^{-1}$] concentration of water vapor in air [kg water vapor (kg air)$^{-1}$]
D	diffusion coefficient [m^2 s^{-1}]
f_p	weighting factor
FT	film thickness [m]
g	gravitational acceleration [m s^{-1}]
h_{fg}	latent heat of vaporization [kJ kg^{-1}]
LH	fin height [m]
LW	fin depth [m]
m	mass flow rate [kg h^{-1}]
M	molecular weight [kg (kg mole)$^{-1}$]
P	pressure [Pa]
RD	rate of dehumidification [kg water h^{-1}]
Re	Reynolds number
RH	relative humidity [%]
RR	rate of regeneration [kg water h^{-1}]
SP	fin spacing [m]
u	solution velocity [m s^{-1}]
V	volume flow rate [m^3 s^{-1}]
w	air velocity [m s^{-1}]
W	humidity ratio [g water vapor (kg dry air)$^{-1}$]
x	coordinate in direction of solution flow [m]
y_1	coordinate from wall in direction perpendicular to solution flow [m]
y_2	coordinate from symmetrical surface in direction perpendicular to the air flow [m]
z	coordinate in direction of air flow [m].

Greek symbols

α	thermal diffusivity [m^2 s^{-1}]
Γ	mass flow rate per fin depth [kg m^{-1} s^{-1}]
δ	liquid film thickness [m]
λ	dimensionless time step
μ	viscosity [kg m^{-1} s^{-1}]
ρ	density [kg m^{-3}].

Subscripts

a	air
f	interface
i	inlet
l	liquid phase
m	model case, or mixture
o	outlet
p	present node
ref	refrigerant
t	TEG solution
v	water vapor
w	water.

gor'eva [9], the temperature entrance zone region is modeled, and the parabolic velocity profile is approximated by a linear profile near the wall and a uniform profile near the interface.

An absorber design was proposed and mathematical models of heat and mass transfer for countercurrent flow were developed by Peng and Howell [10]. Several other regenerator designs have also been proposed and models developed. Andberg and Vliet [11] numerically solved the combined heat and mass transfer in laminar film absorption for a water–LiBr solution.

In Grossman [12], the problem is solved analytically by a series solution and numerically by the method of lines for an isothermal and an adiabatic wall. Grossman and Heath [13] extended the model to account for a turbulent liquid film. The behavior exhibited is similar to that observed in laminar flow. However, the changes in the streamwise direction were more rapid due to the improved transport in turbulent flow. In [14], Grossman studied the diffusion-thermo effect on the film absorption, which is the transport of energy due to concentration gradient. His results showed that in most practical cases the diffusion-thermo effect is quite small.

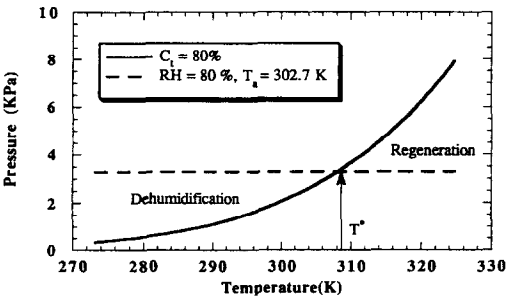

FIG. 1. Comparisons of water vapor pressure in the TEG solution and vapor partial pressure in the ambient air [1].

Kholpanov *et al.* [15] numerically studied combined heat and mass transfer for counterflow of liquid and gas on the basis of solving the conjugate equations of convective mass and energy transfer. Habib and Wood [16] presented numerical solutions for the heat and mass transfer rates in parallel flow film absorption. They proposed new ways to include the gas phase governing equations for this two phase flow problem. Further, they presented numerical solutions for the effect of a nonabsorbable gas on the heat and mass transfer in an open-cycle absorber [17] and in the entrance region of a falling film absorber [18].

EXPERIMENTAL SYSTEM DETAILS

In a hybrid vapor-compression/liquid desiccant air conditioner, liquid desiccant (TEG solution) is dis-

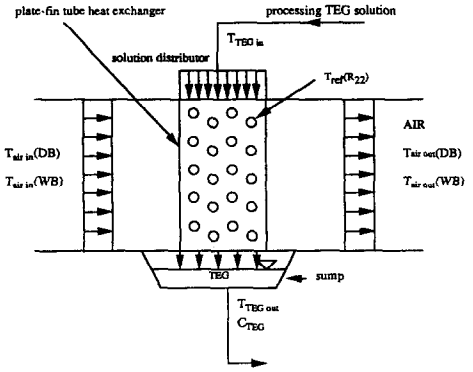

FIG. 2. Experimental test section for condenser (regeneration) or evaporator (dehumidification) of hybrid vapor-compression/liquid desiccant air conditioning system.

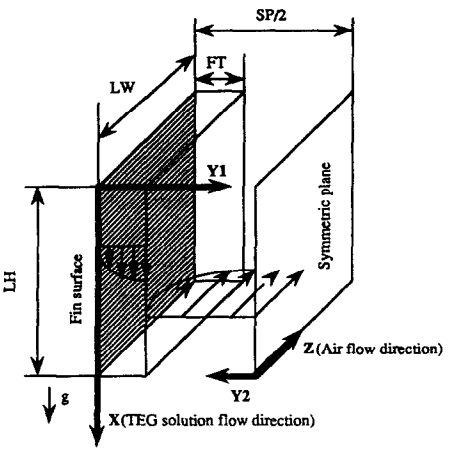

FIG. 3. Schematic diagram for numerical simulation.

tributed over the fins of a plate fin-tube heat exchanger in the absorber (evaporator) and in the regenerator (condenser). The air is blown in cross-flow through the fins to contact the TEG film. Refrigerant is circulated through the tubes of the heat exchanger in the absorber and in the regenerator.

Cooling and dehumidification take place at the same time in the absorber. The refrigerant removes the sensible heat of the air and TEG solution as well as the heat of vaporization released in the absorber. To effectively use waste heat from the vapor-compression refrigeration cycle, the refrigerant is also circulated through the tubes to supply the heat required for regeneration in the regenerator. As the liquid desiccant is heated by refrigerant, water vapor is driven out of solution and carried away by an ambient air stream.

The experimental test section for the absorber and regenerator in this study is shown in Fig. 2 and the characteristics of this fin-tube heat exchanger are given by Table 1. The dry fin characteristics of this heat exchanger are reported by Rich [19]. To determine the performance of the absorber and regenerator, measurements of air and TEG mass flow rates; temperatures of the air, TEG solution, and refrigerant; and TEG concentration are necessary.

For air, the flow-measuring device is an ASME standard venturi with a known discharge coefficient. The TEG flow rates are measured using a rotameter.

Table 1. Configuration of fin-coil heat exchanger used in experiments

Number of rows	4
Number of tubes	$10 \times 4 = 40$
Row arrangement	Staggered
Tube o.d. (after expansion)	0.0133 m (0.525 in)
Fin thickness	1.52E-4 m (0.006 in)
Fin height	0.319 m (12.55 in)
Fin depth	0.111 m (4.35 in)
Tube face spacing	0.0318 m (1.25 in)
Tube row spacing	0.0275 m (1.083 in)
Face width	0.488 m (19.2 in)
Fin pitch	2.63 fins cm^{-1} (6.67 fins in^{-1})

The pressure drop of the venturi is measured with an inclined manometer. The temperature of air, TEG solution, and refrigerant necessary to evaluate the performance of the absorber and regenerator are measured by thermocouples and read using a computer data acquisition system with Labview software. A refractometer is used to determine TEG concentration. The measured input variables are used as input data to the simulation program. Outlet conditions are computed by the program and compared with the values obtained from the experiment.

ANALYSIS

A schematic diagram of the physical model is shown in Fig. 3. The coordinates in the TEG solution flow direction and in the air flow direction are x and z, respectively. The coordinates normal to the wall and from the symmetrical surface are y_1 and y_2, respectively.

The absorber and the regenerator of a hybrid vapor compression/liquid desiccant air conditioner operate in the laminar range [20] of $0 < Re_l < 4$ for a falling film. For laminar flow, the results of Nusselt have been found to accurately predict the thickness and velocity distribution of the film. The resulting film thickness is

$$\delta = \left[\frac{3\Gamma\mu_l}{g\rho_l^2}\right]^{1/3}. \quad (1)$$

The following assumptions are used: the flow is laminar and steady in both liquid and gas; The moist air mixture is an ideal gas; Physical properties in both liquid and gas are constant; Species thermo-diffusion and diffusion-thermo effects are negligible; and thermodynamic equilibrium exists at the air–TEG solution interface.

Governing equations for liquid film

The rate at which vapor is absorbed or desorbed is small compared with the TEG solution flow rate, so

the TEG solution flow rate is constant and therefore its film thickness and mean velocity are also constant. The drag of the gas phase on the liquid film is assumed negligible, so that the velocity gradient in the liquid film at the interface is zero. The velocity profile in the liquid is assumed to be fully developed at the start of the contact length, $x = 0$. Since the rate of absorption is low, the mass flow in the y direction and the associated velocity component v are negligible, and Peclet numbers are large enough that diffusion in the flow direction can be neglected. The presence of the refrigerant tubes is neglected in analyzing the falling film. With these conditions and assumptions, the governing equations become:

x-momentum equation

$$0 = \mu_t \frac{\partial^2 u}{\partial y_1^2} + \rho_t g \tag{2}$$

energy equation

$$u \frac{\partial T_t}{\partial x} = \alpha_t \frac{\partial^2 T_t}{\partial y_1^2} \tag{3}$$

species diffusion equation

$$u \frac{\partial C_w}{\partial x} = D_t \frac{\partial^2 C_w}{\partial y_1^2}. \tag{4}$$

Governing equations for the air flow

The air flows through the small vertical channel between the compact vertical plate fins. The height of the fin plates is much larger than the fin spacing. In addition, the length of the entrance region is very small compared with the total length of the fin plates. The presence of the refrigerant tubes is neglected in treating the air flow. Therefore, the velocity profile in the air flow can be assumed to be fully developed laminar flow between infinite parallel plates.

z-momentum equation

$$0 = -\frac{dp}{dz} + \mu_a \frac{d^2 w}{dy_2^2} \tag{5}$$

energy equation

$$w \frac{\partial T_a}{\partial z} = \alpha_a \frac{\partial^2 T_a}{\partial y_2^2} \tag{6}$$

species diffusion equation

$$w \frac{\partial C_v}{\partial z} = D_a \frac{\partial^2 C_v}{\partial y_2^2}. \tag{7}$$

Boundary and interfacial conditions

The boundary conditions are:

$$\text{at } x = 0, \qquad T_t = T_{ti}; \quad C_w = C_{wi} \tag{8}$$

$$\text{at } z = 0, \qquad T_a = T_{ai}; \quad C_v = C_{vi} \tag{9}$$

$$\text{at } y_1 = 0 \text{ (wall)}, \quad T_t = T_w; \quad \left(\frac{\partial C_w}{\partial y_1}\right)_{y_1 = 0} = 0; \quad u = 0 \tag{10}$$

$$\text{at } y_2 = 0 \text{ (symmetric surface)}, \quad \left(\frac{\partial T_a}{\partial y_2}\right)_{y_2 = 0} = 0;$$

$$\left(\frac{\partial C_v}{\partial y_2}\right)_{y_2 = 0} = 0; \quad \left(\frac{\partial w}{\partial y_2}\right)_{y_2 = 0} = 0 \tag{11}$$

$$\text{at } y_1 = \delta \qquad \left(\frac{\partial u}{\partial y_1}\right)_{y_1 = \delta} = 0 \tag{12}$$

$$\text{at } y_1 = SP/0 \qquad w = 0. \tag{13}$$

The interfacial matching conditions specified at $y_1 = \delta$ or $y_2 = SP/(2-\delta)$ are as follows.

1. Continuity of temperature

$$T_{tf} = T_{af}. \tag{14}$$

2. By assuming the interface to be in thermodynamic equilibrium and the air–vapor mixture to be an ideal gas mixture, the vapor pressure of the water in the TEG solution at the interface is equal to the partial pressure of the water vapor in the air at the interface. The vapor mass fraction in the air can be calculated by [21],

$$C_{vf} = \frac{M_v P_{vf}}{M_a (P_m - P_{vf}) + M_v P_{vf}}, \tag{15}$$

where M_v and M_a represent the molecular weights of the water vapor and air, respectively. P_{vf} is the vapor pressure of water at the interfacial temperature.

The vapor pressure of water in the TEG solution is a function of temperature and concentration. A function fitting the vapor pressure has been derived from data in [1].

$$P_{vf} = f(T_{tf}, C_{wf}). \tag{16}$$

3. Mass balance at the interface

$$\rho_t D_t \frac{\partial C_w}{\partial y_1} = -\rho_a D_a \frac{\partial C_v}{\partial y_2}. \tag{17}$$

4. Energy balance at the interface

$$-k_t \frac{\partial T_t}{\partial y_1} = k_a \frac{\partial T_a}{\partial y_2} + \rho_a D_a \frac{\partial C_v}{\partial y_2} h_{fg}, \tag{18}$$

where h_{fg} is the latent heat of vaporization. Equation (18) indicates that energy exchange between the gas stream and liquid film depends on two related factors: the interfacial temperature gradient on the gas side resulting in sensible heat transfer, and the rate of mass transfer resulting in latent heat transfer. This coupling condition at the interface makes the problem more difficult. An iterative technique must be used, the result of which is to satisfy equations (15)–(18) simultaneously.

Numerical method

Equations (3), (4), (6) and (7) are approximated by finite difference equations using the numerical scheme of Patankar and Baliga [22]. This method has been successfully applied to parabolic boundary-type problems. In this numerical scheme, the axial convection

Table 2. Inlet condition for experiment and computation

Regeneration case 1

C_{ti} (%)	T_{ti} (°C)	W_i	T_{ai} (°C)	V_t (10^{-3} m^3 s^{-1})	V_a (m^3 s^{-1})
76	33.77	21.03	29.56	0.1893	0.1723
78	37.28	20.89	29.44	0.1893	0.1723
80	38.33	21.17	29.67	0.1893	0.1723
82.1	38.89	21.09	29.61	0.1893	0.1723
84	39.44	20.95	29.5	0.1893	0.1723

Regeneration case 2

C_{ti} (%)	T_{ti} (°C)	W_i	T_{ai} (°C)	V_t (10^{-3} m^3 s^{-1})	V_a (m^3 s^{-1})
78	34.51	20.61	29.22	0.1893	0.472
80	34.72	20.75	29.33	0.1893	0.472
82	35.51	20.95	29.51	0.1893	0.472
84	35.94	20.95	29.51	0.1893	0.472

Absorption case 1

C_{ti} (%)	T_{ti} (°C)	W_i	T_{ai} (°C)	V_t (10^{-3} m^3 s^{-1})	V_a (m^3 s^{-1})
75	23.28	20.89	29.44	0.631	0.1416
76	23.67	21.03	29.56	0.631	0.1416
78	24.00	20.95	29.51	0.631	0.1416
80	24.00	20.82	29.61	0.631	0.1416
82	24.72	21.09	29.61	0.631	0.1416
84	25.89	21.09	29.61	0.631	0.1416

Absorption case 2

C_{ti} (%)	T_{ti} (°C)	W_i	T_{ai} (°C)	V_t (10^{-3} m^3 s^{-1})	V_a (m^3 s^{-1})
76	25.39	21.45	29.89	0.631	0.472
78	25.83	21.45	29.89	0.631	0.472
80	25.50	21.02	29.56	0.631	0.472
82	26.44	21.22	29.71	0.631	0.472
84	26.44	21.23	29.72	0.631	0.472

terms in the governing equations for both the liquid solution film and air flow are approximated by upstream differences and the diffusion terms are expressed by central differences with a weighting factor. For the TEG energy equation, for example, the finite difference equation can be expressed as

$$\frac{u(y_1)}{\alpha_t}(T_{t,j,k}^{i+1}-T_{t,j,k}^{i})=\frac{\Delta x}{(\Delta y_1)^2}(T_{t,j+1,k}-2T_{t,j,k}+T_{t,j-1,k}), \tag{19}$$

where

$$T_{t,j,k}=f_jT_{t,j,k}^{i+1}+(1-f_j)T_{t,j,k}^{i} \tag{20}$$

and f_j is a weighting factor which is based on

$$\text{for } 0<\lambda_j<10,\quad f_j=1-\frac{1}{\lambda_j}[1-(1-0.1\lambda_j)^5] \tag{21}$$

$$\text{for } \lambda_j\geqslant 10,\quad f_j=1-\frac{1}{\lambda_j}, \tag{22}$$

where λ_j stands for $2\alpha_t\Delta t/\Delta y^2$ in the heat conduction equation, but for this energy equation, $\Delta x/u$ will be equivalent to Δt [22]. The other equations can be changed in a similar way.

Particular values for f_j lead to the conventional finite-difference schemes; thus $f_j=0$ corresponds to the explicit scheme, $f_j=0.5$ to the Crank–Nicholson scheme, and $f_j=1$ implies the fully implicit scheme. Patankar and Baliga [22] showed that this numerical scheme possesses the accuracy of the Crank–Nicholson method for small steps, the physical realism of the fully implicit method for large steps in the marching coordinate, and the stability of both.

Each system of the finite-difference equations forms a tridiagonal matrix equation, which can be efficiently solved using the Thomas algorithm [23]. Algebraic transformations for governing equations are used to cluster grid points in inlet regions to handle large changes of temperature and concentration [23].

The following is a brief outline of the solution procedure for given conditions.

(a) Initialize the input variables such as inlet and boundary conditions.

(b) Calculate the film thickness and change the marching coordinate by an algebraic transformation relation.

(c) Assume the interface temperature.

(d) Calculate the wall temperature by using a heat resistance relation for the refrigerant, fin, and liquid film.

(e) Solve the tridiagonal matrix representing the energy equation.

(f) Assume the TEG concentration at the interface and evaluate the vapor concentration of the air by using the interface thermodynamic equilibrium condition.

(g) Solve the mass diffusion equations.

(h) Check if the assumed TEG concentration satisfies the mass balance at the interface. If not, repeat procedures (f)–(h).

(i) Check if the energy balance at the interface, equation (16), is satisfied. If not, recalculate the interface temperature based on equation (18) and repeat procedures (c)–(i). If yes, proceed to the next marching location and apply procedures (c)–(i).

The results of the numerical analysis are detailed three-dimensional profiles of concentration and temperature in both the TEG and air streams. The profiles are averaged over the outlet streams in order to compare with the measured experimental results, which were mixed-mean values. More details of the method are given in Park *et al.* [24].

RESULTS AND DISCUSSIONS

The performance of the regenerator may be described by the regeneration rate and the outlet con-

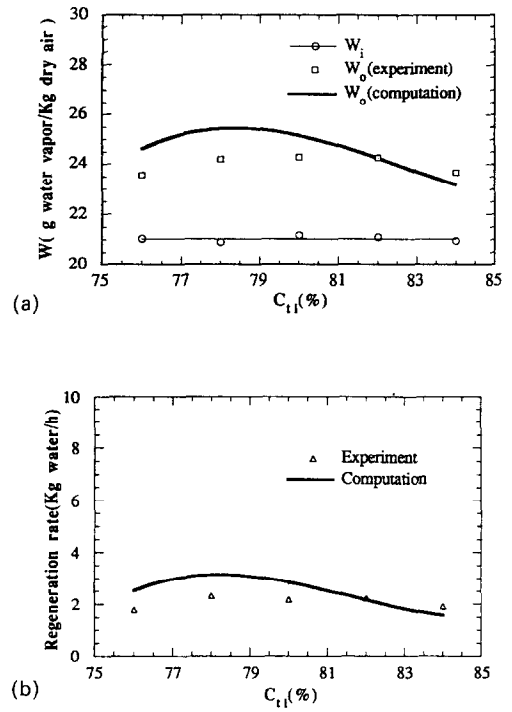

FIG. 4. Comparison of computational and experimental results for regeneration: Case 1 [$V_{a,m} = 0.172$ m^3 s^{-1} ($=365$ cfm), $V_{t,m} = 0.189 \times 10^{-3}$ m^3 s^{-1} ($= 3.0$ gpm)]. (a) Air humidity ratio for regeneration (Case 1). (b) Total regeneration rate of regenerator (condenser) (Case 1).

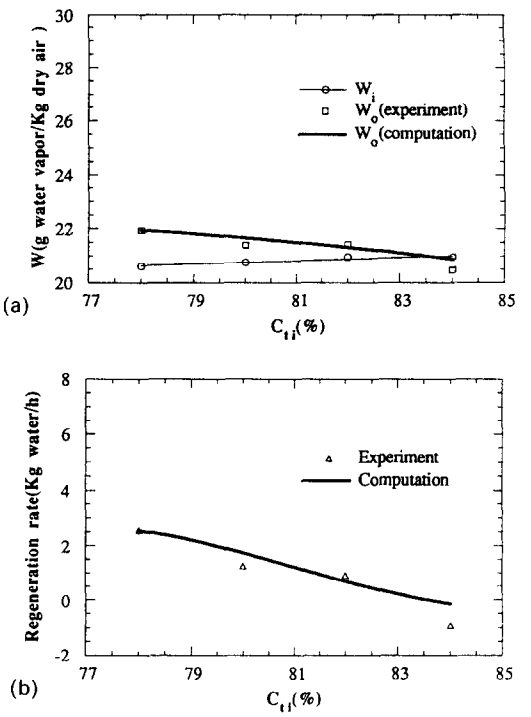

FIG. 5. Comparison of computation and experimental results for regeneration: Case 2 [$V_{a,m} = 0.472$ m^3 s^{-1} ($= 1000$ cfm), $V_{t,m} = 0.189 \times 10^{-3}$ m^3 s^{-1} ($= 3.0$ gpm)]. (a) Air humidity ratio for regeneration (Case 2). (b) Total regeneration rate of regenerator (condenser) (Case 2).

centration of the desiccant, while the performance of the absorber is described by the absorption rate and the outlet humidity ratio and temperature of the air. These are influenced by climatic and operational variables such as temperature and humidity of the ambient air, inlet temperature and concentration of TEG solution, and air and solution flow rates. The input variables measured during the experiments are used as input values to the simulation program, and the outlet conditions are computed by the program and compared.

Figure 4 compares the computed and experimental results for regeneration case 1. This case has the lowest air flow rate for a given TEG solution flow rate. Outlet humidity ratio and total regeneration rate for the same air inlet condition decrease at higher TEG inlet concentrations. Total regeneration rates can be calculated from the expression

$$m_w = m_a(W_o - W_i) \tag{23}$$

which gives the amount of water transferred from the solution to the air. At lower TEG concentrations, the interfacial humidity of the liquid is greater. The driving force for mass transfer during regeneration decreases more rapidly at higher concentrations for a given temperature, which results in lower regeneration rates at higher TEG concentration.

Figure 5 shows the results for the same TEG flow rate as in Fig. 4 but at increased air flow rate. This figure shows the decrease of regeneration rate compared with regeneration case 1 for lower air flow rate. That is to say, for regeneration, the lower air flow rate gives better regeneration performance than does the higher air flow rate. In this figure we note that at higher concentration, absorption occurs instead of regeneration for this high inlet humidity condition. This effect is caused by the lower inlet TEG temperature used in case 2.

Figure 6 shows the psychrometric comparison of both of the regeneration cases for $C_{ti} = 76\%$. In the figure we note that the lower air flow rate case has much better regeneration characteristics than the higher air flow rate case. Computational results show

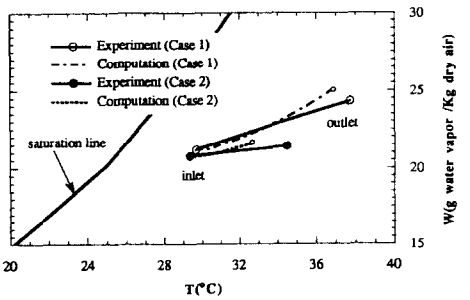

FIG. 6. Psychrometric comparison of computational and experimental results for regeneration ($C_{ti} = 76\%$).

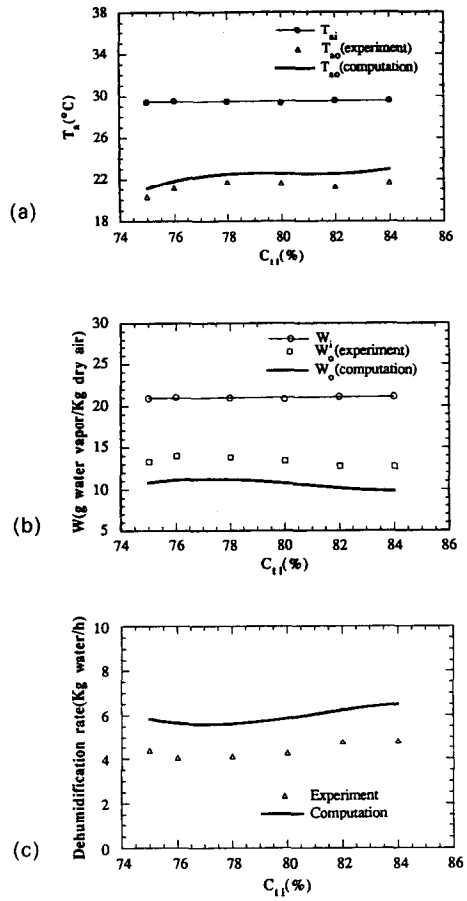

FIG. 7. Comparison of computational and experimental results for absorption: Case 1 [$V_{a,m} = 0.142$ m^3 s^{-1}(= 300 cfm), $V_{t,m} = 0.631 \times 10^{-4}$ m^3 s^{-1}(= 1.0 gpm)]. (a) Air temperature for absorption (Case 1). (b) Air humidity ratio for absorption (Case 1). (c) Total dehumidification rate of absorber (evaporator) (Case 1).

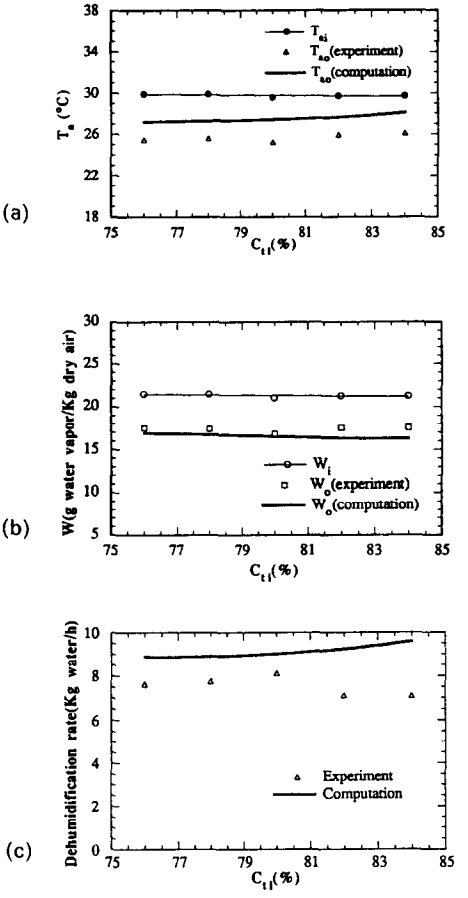

FIG. 8. Comparison of computational and experimental results for absorption: Case 2 [$V_{a,m} = 0.472$ m^3 s^{-1}(= 1000 cfm), $V_{t,m} = 0.631 \times 10^{-4}$ m^3 s^{-1}(= 1.0 gpm)]. (a) Air temperature for absorption (Case 2). (b) Air humidity ratio for absorption (Case 2). (c) Total dehumidification rate of absorber (evaporator) (Case 2).

a little higher outlet humidity ratio and lower dry bulb temperature; in other words, higher mass transfer and lower heat transfer than observed in the experiment. This probably occurs because in the calculation we assumed that the TEG solution film is wetting the fin completely, which may not occur in the experiment. Therefore, the TEG solution film is assumed to cover a larger surface area for mass transfer than occurs in the experiment (where part of the surface of the fin is covered by the refrigerant tubes, and part of the fin may not be wetted). Also, in the experiments, the bare refrigerant tubes play a significant role in heat transfer.

Figures 7 and 8 show two cases of absorption, where TEG flow rates are the same but the air flow rates differ. Figures 7(a) and 8(a) show the air-cooling effect for different air flow rates with the same TEG flow rate. As is expected, the cooling effect decreases with higher air flow rate. From Figs. 7(b) and 8(b), we note that for a given TEG concentration the difference between inlet and outlet humidity ratio for the lower air flow rate case is greater than that of higher air flow rate case. For the lower air flow rate case, moist air has more contact time with the film solution. However, the total sensible heat transfer from the air to the TEG solution is smaller than for the higher air flow rate.

Figures 7(c) and 8(c) show the total absorption rate for different air flow rates. Computated results have the same trends as the experimental results but generally predict better dehumidification. This can be explained in a similar manner as for regeneration. Figure 9 shows the psychrometric comparison of the absorption case. The lower air flow rate case clearly shows better humidity control and air cooling. This figure implies that air flow rate should be controlled to get the desired outlet air temperature and humidity.

CONCLUSIONS

A numerical model is developed for analysis of the combined heat and mass transfer between laminar liquid desiccant films and air in cross-flow. The results

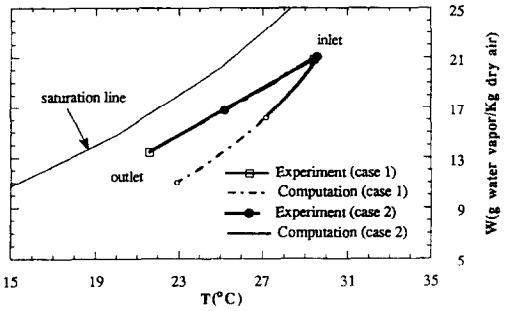

FIG. 9. Psychrometric comparison of computational and experimental results for absorption ($C_{ti} = 80\%$).

of the numerical prediction compare quite well with experimental results. Lower air flow rates provide better humidity control and air cooling over the range investigated.

That the computational results show the same trends as the experimental results indicates that this numerical analysis can be used for parametric analysis for air–liquid desiccant cross-flow systems.

Acknowledgements—The authors wish to acknowledge support for this work from the State of Texas Higher Education Coordinating Board under the Energy Research Applications Program grant ERAP #086.

REFERENCES

1. *Triethylene Glycol*. Union Carbide Corporation, New York (1989).
2. G. Ameringer, Experimental and theoretical analysis of an absorber for a liquid desiccant solar air-conditioning system, MS Thesis, The University of Texas at Austin, Austin, Texas (1982).
3. G. D. Fulford, The flow of liquids in thin films, In *Advances in Chemical Engineering*, Vol. 5, pp. 151–236 (1964).
4. W. E. Olbrich and J. D. Wild, Diffusion from the free surface into a liquid film in laminar flow over defined shapes, *Chem. Engng Sci.* **24**, 25–32 (1969).
5. A. Tamir and Y. Taitel, Diffusion to flow down an incline with surface resistance, *Chem. Engng Sci.* **26**, 799–808 (1971).
6. Z. Rotem, and J. E. Neilson, Exact solution for diffusion flow down an incline, *Canadian J. Chem. Engng* **47**, 341–346 (1969).
7. N. S. Murty and V. M. K. Sastri, Accelerating laminar liquid film along a inclined wall, *Chem. Engng Sci.* **28**, 869–874 (1973).
8. N. I. Grigor'eva and V. E. Nakoryakov, Exact solution of combined heat- and mass-transfer problem during film absorption, *J. Engng Phys* **33** (5), 1349–1353 (1977).
9. V. E. Nakoryakov and N. I. Grigor'eva, Combined heat and mass transfer in film absorption, *Heat Transfer—Sov. Res.* **12**(3), 111–117 (1980).
10. C. S. P. Peng and J. R. Howell, Analysis and design of efficient absorbers for low-temperature desiccant air conditioners, *J. Solar Energy Eng* **103**, 67–74 (1981).
11. J. C. Andberg and G. C. Vliet, Nonisothermal absorption of gases into falling liquid films, *ASME—JSME Thermal Engng Joint Conf.*, Vol. 2, pp. 423–431 (1983).
12. G. Grossman, Simultaneous heat and mass transfer in film absorption under laminar flow, *Int. J. Heat Mass Transfer* **26**, 357–371 (1983).
13. G. Grossman and M. T. Heath, Simultaneous heat and mass transfer in absorption of gases in turbulent liquid films, *Int. J. Heat Mass Transfer* **27**(12), 2365–2376 (1984).
14. G. Grossman, Analysis of diffusion thermo-effects in film absorption, *Proc. 8th Int. Heat Transfer Conf.*, Vol. 4, pp. 1977–1982 (1986).
15. L. P. Kholpanov, E. Ya. Kenig and V. A. Malyusov, Combined heat and mass transfer for opposing film flows of liquid and gas, *J. Engng Phys* **51**, 768–773 (1986).
16. H. M. Habib and B. D. Wood, Simultaneous heat and mass transfer for a falling film absorber—The two phase flow problem, *Proc. of 12th annual ASME Solar Energy Conf.*, pp. 61–67 (1990).
17. H. M. Habib, B. D. Wood and J. Y. Murty, Effect of non-absorbable gas on the performance of a falling film absorber for open-cycle absorption solar cooling system, *Proc. of 11th annual ASME Solar Energy Conf.*, pp. 247–255 (1989).
18. H. M. Habib, T. A. Ameel and B. D. Wood, Effects of a non-absorbable gas on the heat and mass transfer for the entrance region of a falling film absorber, *Proc. of 13th annual ASME Solar Energy Conf.*, pp. 475–481 (1991).
19. D. G. Rich, The effect of fin spacing on the heat transfer and friction performance of multi-row, smooth plate fin-and-tube heat exchangers, *ASHRAE Trans. P.* 2, pp. 137–145 (1973).
20. R. B. Bird, W. E. Stewart and E. N. Lightfoot, *Transport Phenomena*, Wiley, New York (1960).
21. C. J. Chang, T. F. Lin and W. M. Yan, Natural convection flows in a vertical, open tube resulting from combined buoyancy effects of thermal and mass diffusion, *Int. J. Heat Mass Transfer* **29**, 1543–1552 (1986).
22. S. V. Patankar and B. R. Baliga, A new-finite difference scheme for parabolic differential equations, *Numer. Heat Transfer* **1**, 27–37 (1978).
23. D. A. Anderson, J. C. Tannehill and R. H. Pletcher, *Computational Fluid Mechanics and Heat Transfer*, McGraw-Hill, New York (1984).
24. M. S. Park, G. C. Vliet and J. R. Howell, Coupled heat and mass transfer between a falling desiccant film and air in cross-flow: II—Parametric analysis and results, *AIAA/ASME Thermophys. Heat Transfer Conf.*, Colorado Springs (1994).